

## Topological phases of strongly interacting time-reversal invariant topological superconducting chains under a magnetic field

Leandro M. Chinellato <sup>1</sup>, Claudio J. Gazza <sup>1</sup>, Alejandro M. Lobos,<sup>2,3,\*</sup> and Armando A. Aligia <sup>4</sup>


<sup>1</sup>*Instituto de Física Rosario, CONICET, and Facultad de Ciencias Exactas, Ingeniería y Agrimensura, Universidad Nacional de Rosario, 2000 Rosario Argentina*

<sup>2</sup>*Instituto Interdisciplinario de Ciencias Básicas - Consejo Nacional de Investigaciones Científicas y Técnicas, Padre Jorge Contreras 1300, Parque General San Martín, M5502JMA, Mendoza, Argentina*

<sup>3</sup>*Facultad de Ciencias Exactas y Naturales - Universidad Nacional de Cuyo,*

*Padre Jorge Contreras 1300, Parque General San Martín, M5502JMA, Mendoza, Argentina*

<sup>4</sup>*Instituto de Nanociencia y Nanotecnología CNEA-CONICET, GAIDI, Centro Atómico Bariloche and Instituto Balseiro, 8400 Bariloche, Argentina*

 (Received 27 October 2023; revised 16 January 2024; accepted 18 January 2024; published 8 February 2024)

Using the density-matrix renormalization group, we determine the different topological phases and low-energy excitations of a time-reversal invariant topological superconducting (TRITOPS) wire with extended  $s$ -wave superconductivity, Rashba spin-orbit coupling (SOC) and on-site repulsion  $U$ , under an externally applied Zeeman field  $J$ . For the case in which  $J$  is perpendicular to the SOC, the model describes a chain of Shiba impurities on top of a superconductor with extended superconductor pairing. We identify the different topological phases of the model at temperature  $T = 0$ , and in particular we study the stability of the TRITOPS phase against the Zeeman field  $J$  and the chemical potential  $\mu$ , for different values of  $U$ . In the case where the magnetic field  $J$  is perpendicular to the SOC axis, the pair of Kramers degenerate Majorana zero modes at the edges of the system that exist for  $J = 0$ , remain degenerate until a critical value of the magnetic field is reached. For  $J$  parallel to the SOC and up to moderate values of  $U$ , the fractional spin projection  $\langle S_y \rangle = 1/4$  at the ends, found for noninteracting wires at  $U = 0$ , is recovered. In addition, the analytic expression that relates  $\langle S_y \rangle$  with  $J$  for finite noninteracting chains is shown to be universal up to moderate values of  $U$ .

DOI: [10.1103/PhysRevB.109.064503](https://doi.org/10.1103/PhysRevB.109.064503)

### I. INTRODUCTION

The quest for topological phases of matter and, in particular, topological superconductors (TOPS) has been a major pursuit in condensed matter physics for the last 20 years [1]. TOPS phases hosting elusive Majorana zero modes (MZMs) have attracted a lot of interest both from the fundamental point of view, as well as for potential uses in fault-tolerant quantum computation due to their exotic non-Abelian anyonic statistics [2].

Although much of the progress in this area has been achieved within a framework of noninteracting electrons (i.e., the topological classification of TOPS phases according to their symmetries and the identification of possible topological invariants), the effects of interactions still remains as a conceptually important open question. Moreover, many of the technologically relevant applications might involve low-dimensional TOPS systems, for which the effects of interactions are enhanced [3]. Therefore, the study of interaction effects on TOPS is also relevant from the technological perspective.

Up to now, a variety of different physical systems have been proposed to realize TOPS phases hosting MZM states:  $\nu = 5/2$  fractional quantum Hall state [4], superfluid

He-3 [5], proximitized topological insulator-superconductor structures [6], superconducting heterostructures combining proximity-induced superconductivity, semiconductors with strong Rashba spin-orbit interaction and Zeeman fields [7–9], etc. All these systems are potential realizations of TOPS phases, which break time-reversal symmetry (“class D” TOPS in the Altland-Zirnbauer classification [10,11]).

A different class, the time-reversal invariant TOPS (TRITOPS) or DIII class TOPS originally proposed by Qi *et al.* [12,13], has been predicted by Zhang, Kane, and Mele (ZKM) to arise in 1D or 2D geometries by combining semiconductors with strong Rashba spin-orbit coupling (SOC) (i.e., nanowires or films) proximitized with extended  $s$ -wave superconductors [14]. The TRITOPS have been recently the subject of intense theoretical research [12–29]. For 1D TRITOPS, a key feature is the existence of Kramers pairs of MZMs at the edges of the system. Another peculiar feature is that the spin projection at the ends in the direction of the SOC is  $\pm 1/4$  [12,21,25]. For a TRITOPS wire of length  $L$ , MZMs are well defined as long as  $L \gg \xi$ , with  $\xi$  the MZM localization length. Under these conditions, an external magnetic field applied to *one-half* of the wire in the direction of the SOC produces a Zeeman-split pair of low-energy MZMs with total spin projection at the end equal to  $1/4$  or  $-1/4$ , depending on the sign of the magnetic field [21,25].

The effect of repulsive interactions in 1D TOPS and TRITOPS has been studied in previous works using e.g.,

\*alejandro.martin.lobos@gmail.com

mean-field approaches [30], density-matrix renormalization group (DMRG) [18,27,28], the Abelian bosonization framework [31], and numerical renormalization group for two sites [32]. While for 1D TOPS interactions tend to weaken the superconducting correlations, therefore weakening the TOPS phase [33,34], it was suggested that repulsive interactions in a 1D system stabilizes the TRITOPS phase. The basic stabilization mechanism consists in local repulsive interactions, which penalize the proximity-induced singlet pairing with respect to the proximity-induced triplet pairing [31,35]. In addition, although it is not the scope of the present paper, we mention in passing that the effect of attractive interactions on TRITOPS has also been studied [36].

In this article we explore the effects of on-site repulsive interaction  $U$  on the ZKM model in the presence of a magnetic field  $J$ . For  $J$  perpendicular to the SOC, the model describes hybrid magnet-superconductor systems with TOPS and TRITOPS phases, in particular magnetic adatoms (i.e., Fe, Co, or Mn atoms) deposited on top of a superconductor, a system usually known as a ‘‘Shiba chain’’. Recent experimental progress in these type of hybrid nanostructures have shown preliminary evidence of MZMs in the  $dI/dV$  STM signal [37–43], drawing a lot of interest. However, the small size of the parent superconductor gap (typically Pb) imposes practical difficulties in all type of proximity-induced TOPS, such as, e.g., stringent low-temperature requirements and limited spectral resolution of the experiments. For this reason, recent theoretical proposals have put forward the possibility to observe both TOPS and TRITOPS in nanostructures made of magnetic impurities deposited at the surface of unconventional high- $T_c$  superconductors, generating renewed interest on these hybrid structures [44].

In this paper, using the density-matrix renormalization group (DMRG) method, we study the topological phase diagram of the system for finite magnetic field perpendicular to the SOC and for different values of  $U$ . We also explore the response of the MZMs to the presence of a magnetic field applied to one half of the chain. Such a magnetic probe can help to detect and identify the topological phase of the chain. In particular, we show that the fractional spin  $1/4$  excitations at each end of the wire, predicted to emerge in noninteracting models for magnetic field parallel to the SOC [12,21,25], are robust to the presence of strong interactions.

The paper is organized as follows. In Sec. II we explain our model. Section III contains the main results and Sec. IV is a summary and discussion.

## II. THEORETICAL MODEL AND METHODS

We consider the following discrete Hamiltonian encoding the minimal ingredients leading to a TRITOPS phase (in close analogy to the ZKM model in the continuum), with additional Zeeman and an on-site repulsion terms,

$$H = \sum_j \left[ \left( t c_j^\dagger c_{j+1} - \left( \frac{\mu}{2} + \frac{U}{4} \right) c_j^\dagger c_j + \Delta c_{j,\uparrow}^\dagger c_{j+1,\downarrow}^\dagger + i\alpha_R c_j^\dagger \sigma_y c_{j+1} + \text{H.c.} \right) - J c_j^\dagger \sigma_\beta c_j + U n_{j,\uparrow} n_{j,\downarrow} \right] \quad (1)$$

where  $\mathbf{c}_j^\dagger = (c_{j,\uparrow}^\dagger, c_{j,\downarrow}^\dagger)$  is a spinor containing both fermionic creation operators at site  $j$  with spin projections  $\{\uparrow, \downarrow\}$ ,  $\sigma_\alpha$  (with  $\alpha = \{x, y, z\}$ ) are the  $2 \times 2$  Pauli matrices,  $t$  is the nearest-neighbor-hopping amplitude,  $\mu$  is the chemical potential,  $\alpha_R$  is the Rashba SOC in the  $y$  direction,  $\Delta$  is the extended  $s$ -wave amplitude of the superconducting first-neighbor pairing correlations, and  $U$  is the on-site electron-electron repulsion. This particular form of Eq. (1) ensures that for any value of  $U$ ,  $\mu = 0$  corresponds to the particle-hole symmetric point.

While the presence of a nearby bulk superconductor usually screens the electron-electron interaction, in low-dimensional nanostructures of reduced dimensions, local repulsion terms of this type might be relevant, and in fact (as we show below) this is the case for the ground-state phase diagram of this system. In the above model, the Zeeman parameter  $J$  can either represent the effect of an external magnetic field ( $J = \mu_B B$ ), where  $\mu_B$  is the Bohr magneton, applied along the  $\beta$  direction, or (in the case of atomic Shiba chains) the effect of a local exchange field originated in a microscopic  $s$ - $d$  exchange interaction  $I_{sd}$  ( $J = 2I_{sd}S_z^j$ ) between the conduction states and the magnetic impurities  $S_z^j$  assumed ferromagnetically aligned along  $z$  at each site  $j$  of the chain. In this case,  $\beta = z$  and the effect is similar to a magnetic field perpendicular to the SOC. We will also consider the case when  $J$  is parallel to the SOC ( $\beta = y$ ).

All the numerical results presented in this paper have been obtained by the means of DMRG computations, implemented using the ITensor software library [45]. We have implemented the necessary maximum bond dimension (400 in the worst case), which allowed us to keep the truncation error cutoff of  $10^{-10}$  throughout.

## III. RESULTS

### A. Topological phase diagram

We now focus on the ground-state properties of the system and study the topological phase diagram as a function of the chemical potential  $\mu$  and the Zeeman field  $J$  perpendicular to the SOC, for different values of the interaction parameter  $U$  (see Fig. 1). The other parameters of the model are fixed throughout the rest of the paper to the values  $\Delta = 1.2$ ,  $\alpha_R = 0.8$  (here the hopping amplitude  $t = 1$  has been chosen as the unit of energy). This particular parameter set has been chosen to coincide with those used in Ref. [44].

While topological invariants of strongly correlated systems have been calculated using Green’s functions [46,47], or extensions of the Zak’s Berry phase [48], they present serious difficulties to be implemented with DMRG. Therefore, we determine the topological nature of the ground state by analyzing the degeneracy of the reduced density-matrix entanglement spectrum [49,50]. Given a quantum system, which can be divided into two subsystems  $A$  and  $B$ , the entanglement spectrum is the spectrum of eigenvalues of the reduced density matrix  $\rho_A$  ( $\rho_B$ ), obtained after tracing out the  $B$  ( $A$ ) degrees of freedom. The change of degeneracies in the entanglement spectrum is indicative of topological quantum phase transitions occurring in the ground state of the whole system, and is related to the degeneracy of the ground state and the number of MZMs per end of the chain [49,50].

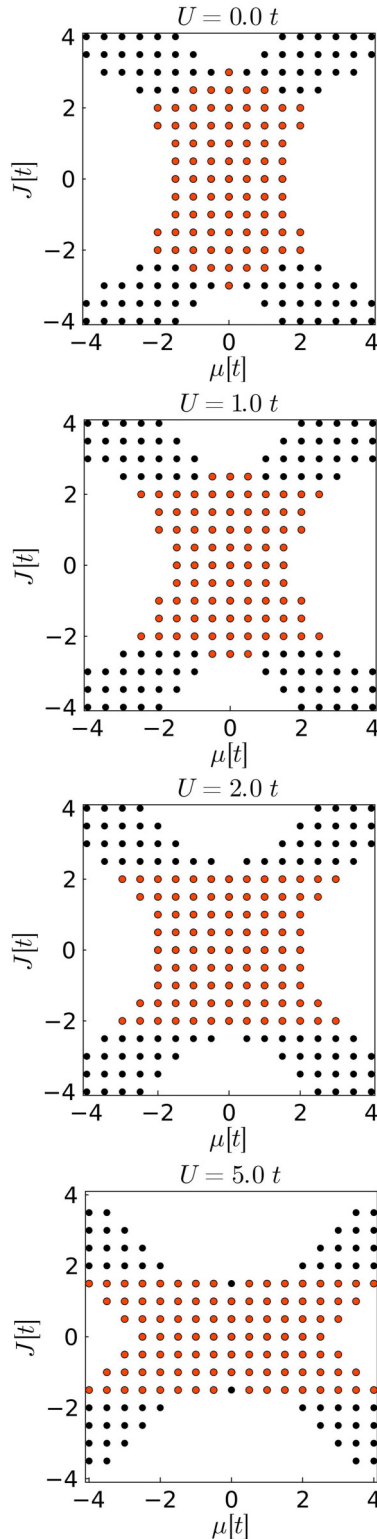


FIG. 1. Topological phase diagram as a function of chemical potential and magnetic field perpendicular to the SOC. Red (black) dots correspond to fourfold (twofold) degeneracy of the entanglement spectrum. Parameters are  $\Delta = 1.2$  and  $\alpha = 0.8$ , and the length of the chain is  $L = 400$  sites.

Generically speaking, starting from a parameter regime, which realizes a time-reversal symmetric superconductor [ $J = 0$  in our model Eq. (1)] and for low or moderate values of

$\mu$ , we obtain a fourfold degenerate ground state indicative of a TRITOPS phase (red dots in Fig. 1). Interestingly, we see that this phase is robust against the effect of a uniform magnetic field perpendicular to the SOC, and only for quite large values of  $J$  beyond a critical line  $J_c(\mu)$  the system becomes a DIII TOPS with a twofold degenerate ground state (see black dots). Additionally, for extremely low (large) values of  $\mu$ , the bands can be completely depleted (filled) and the system becomes a trivial insulator with a nondegenerate ground state (white region in Fig. 1).

The aforementioned robustness of the fourfold ground-state multiplet is quite surprising given the fact that time-reversal symmetry no longer protects the TRITOPS phase. In the noninteracting case, this is related to the presence of an additional chiral symmetry, implemented by the operator  $\mathcal{S} = \sigma_y \tau_y$  (where the Pauli matrices  $\tau_\alpha$  operate on the Nambu space), which anticommutes with  $H$ . Indeed, for  $U = 0$ , and taking periodic boundary conditions in Eq. (1), the Hamiltonian matrix of the system takes the compact form in  $k$  space  $\mathcal{H}_k = (\epsilon_k - \mu)\sigma_0\tau_z + \alpha\sigma_y\tau_z + \Delta_k\sigma_0\tau_x + J\sigma_\beta\tau_0$ , where the Nambu basis  $\Psi_k = (c_{k\uparrow}, c_{c,\downarrow}, c_{-k\downarrow}^\dagger, -c_{-k\uparrow}^\dagger)^T$  has been used, and where  $\epsilon_k = 2t \cos(k)$  and  $\Delta_k = \Delta \cos(k)$ . It is easy to see that when  $\beta = z$  the chiral operator  $\mathcal{S}$  anticommutes with  $\mathcal{H}_k$ , and generates a chiral symmetry, which is *additional* to the time-reversal symmetry occurring for  $J = 0$ . This additional symmetry allows to compute a  $Z$  invariant, which counts the number of MZMs at each end of the wire [51].

On the other hand, as can be seen in Fig. 1, the presence of a local on-site interaction Hubbard  $U$  term has an important effect on the topological phase diagram, as it tends to weaken the TRITOPS phase with respect to the magnetic field. This effect can be qualitatively understood in terms of an effective noninteracting model with a smaller renormalized superconducting bulk gap due to the repulsive interaction. In the following we denote this gap excluding the low-energy excitations related with the MZMs as  $\Delta_s$ . This gap is calculated as follows. The one-particle excitation energies are defined as the different energies in the subspace with odd number of particles minus the ground-state energy (which lies in the subspace with even number of particles)

$$E_n = E_n^{(\text{odd})} - E_g^{(\text{even})}, \quad (2)$$

where the subscript  $g$  denotes the ground state. Among these  $E_n$ , in the topologically nontrivial regions, there is a low-lying subset, which correspond to the MZMs, with a small exponential splitting  $\sim e^{-L/\xi}$  for a finite chain, due to the mixing of the MZMs between both ends. The corresponding excitation energies of this subset behave as  $E_n \rightarrow 0$  for  $L \rightarrow \infty$ , and can be easily identified with a finite-size scaling analysis. The next excitation energy above this multiplet defines  $\Delta_s$ , which can be identified with bulk excitations. In Fig. 2, we show  $\Delta_s$  as a function of on-site repulsion. One can clearly see that the value of  $\Delta_s$  decreases by nearly a factor 2 as  $U$  increases from 2 to 6. The detrimental effects of the repulsive interactions on  $\Delta_s$  allows to qualitatively understand the topological phase diagram on Fig. 1. In the inset of Fig. 2, we show the aforementioned low-lying multiplet of MZMs, and the bulk-excitation gap  $\Delta_s$  (for which no appreciable dependence of  $\Delta_s \sim 0.58$  on the length of the chain  $L$  is observed), computed for the particular value  $U = 6$ .

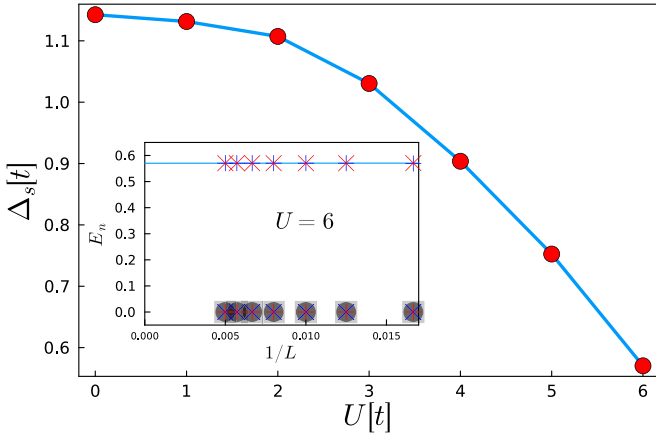


FIG. 2. Superconducting single-particle excitation gap  $\Delta_s$  (defined in the main text) computed for several values of  $U$ , and for  $\mu = J = 0$ . (Inset) Finite-size scaling showing the first excitations in the odd-parity subspace for  $U = 6$ .

This renormalization of  $\Delta_s$  due to the repulsion  $U$  has detrimental effects on the stability of the TRITOPS phase, in particular when  $J$  is increased (see Fig. 1). Note, however, that increasing  $U$  also strengthens the TRITOPS phase with respect to the chemical potential  $\mu$ . An intuitive way to understand this effect is obtained using the framework of the mean-field approximation: Decoupling the interaction in the density-density channel, i.e.:  $Un_{j,\uparrow}n_{j,\downarrow} \rightarrow U[n_{j,\uparrow}\langle n_{j,\downarrow} \rangle + \langle n_{j,\uparrow} \rangle n_{j,\downarrow} - \langle n_{j,\uparrow} \rangle \langle n_{j,\downarrow} \rangle]$  has the effect of renormalizing the single-particle spectrum to  $\epsilon_k \rightarrow \tilde{\epsilon}_k = \epsilon_k + U(\langle n \rangle - 1)/2$ , where we have reasonably assumed an homogeneous and paramagnetic solution  $\langle n_{j,\uparrow} \rangle = \langle n_{j,\downarrow} \rangle = \langle n \rangle/2$ , and where  $\epsilon_k$  is the noninteracting dispersion. Then, for  $\mu > 0$  when the total occupation per site is  $\langle n \rangle > 1$ , a larger value of  $\mu$  is necessary to compensate for the interaction-induced depletion of the renormalized band and, therefore, to obtain the same value of the 1D TRITOP topological invariant (see e.g., Ref. [12]) as compared to the noninteracting case. The opposite occurs for  $\mu < 0$ , and a lower value of  $\mu$  is necessary. This effectively extends the stability region of the TRITOPS phase near the line  $J = 0$  with respect to  $\mu$ , a fact that could be beneficial to stabilize TRITOPS phases in potential implementations in devices. Indeed, by changing the parameters of the model, we can go from either a TRITOPS with fourfold degeneracy of the ground state, to a D-class topological phase with twofold degeneracy, to a trivial superconducting phase with a nondegenerate ground state.

As a way to characterize the different phases of the model, in the next sections we consider an inhomogeneous Zeeman term applied to one half of the system (i.e., the left half). The introduction of a time-reversal symmetry-breaking interaction to only one end of the system allows to phenomenologically characterize the behavior of the MZMs arising in TRITOPS.

### B. Magnetic field at the end perpendicular to the SOC

In this section we explore the fate of the MZMs in the TRITOPS phase when a magnetic field perpendicular to the SOC is applied to the left part of the chain [Eq. (1) with a term  $-J \sum_{j=1}^{L/2} \mathbf{c}_j^\dagger \sigma_z \mathbf{c}_j$ ]. To that end we begin with the study

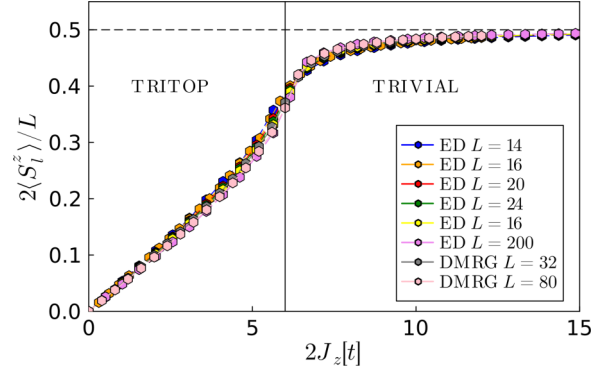


FIG. 3. Magnetization at the left side of the noninteracting ( $U = 0$ ) chain as a function of magnetic field applied to the left half of the chain. The different data sets represent different lengths  $L$ . The parameters set is  $t = 1$ ,  $\Delta = 1.2$ ,  $\alpha = 0.8$ , and  $\mu = U = 0$ .

of the noninteracting case  $U = 0$ , where exact calculations independent of the DMRG procedure are available, and compute the magnetization of the left half of the chain  $S_l^z = \sum_{j=1}^{L/2} S_j^z$ .

In the topological phases and for low values of  $J$ , one expects the magnetization to be dominated by the MZMs, which are localized near both ends of the chain. For this reason, the spatial extension of the magnetic field is not important as long as it is longer than the MZM localization length  $\xi$ . However, rather surprisingly, for a magnetic field perpendicular to the SOC, the Kramers-degenerate MZMs of the TRITOPS are not mixed by the magnetic field [21]. This is related to the additional chiral symmetry  $S = \sigma_y \tau_y$  mentioned above. The leading correction to the ground-state energy becomes of second order in  $J$  (i.e., quasiparticles are excited into the bulk and then return to the ground state), leading to a linear dependence of  $\langle S_l^z \rangle$  with  $J$ . This is in fact the behavior observed for small  $J$ , displayed in Fig. 3. The slope is a fraction of  $J/\Delta_s$ , where  $\Delta_s$  is the superconducting gap, as expected for bulk excitations. For  $U = 0$ , the model can be solved exactly without using DMRG and we used these calculations to check our DMRG results. Note that all the plots eventually saturate at the value  $1/2$ , corresponding to the completely polarized ground state, as is physically expected for very large values of the magnetic field.

In Fig. 4 we show the changes introduced by a variation of the chemical potential. For  $\mu \geq 2$  the system enters the trivial phase and the MZMs disappear. Therefore, the effect of the magnetic field is much weaker for small  $J$ . However, for large  $\mu$ , increasing  $J$  the system enters the topological phase with one MZM at each end (black dots in Fig. 1) and  $\langle S_l^z \rangle$  increases in that region (for example for  $2.6 < J/t < 9.4$  for  $\mu = 2.5$ ) before reentering the trivial phase for large  $J$ , where  $\langle S_l^z \rangle$  saturates at the value  $1/2$ . We think that the change in slope of the curve for  $\mu = |t|$  at  $J_z \sim 4|t|$  is related to the TOPS-trivial transition, while the corresponding changes for  $\mu > 2|t|$  are related to the opposite transition (see Fig. 1).

Finally, in Fig. 5 we explore the effect of a finite  $U$ . As discussed in Sec. I, the gap  $\Delta_s$  decreases with increasing  $U$  and therefore the slope of  $\langle S_l^z \rangle$  for small  $J$ , which is expected to be inversely proportional to  $\Delta_s$  increases. This behavior

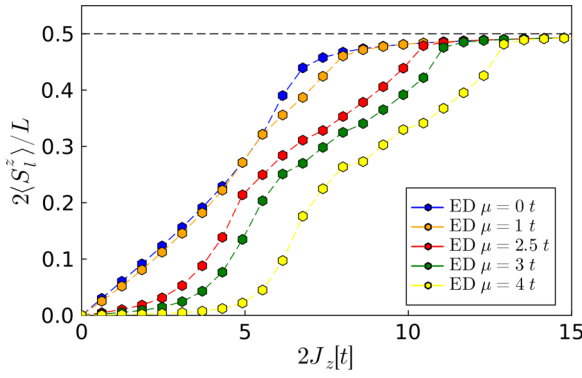


FIG. 4. Magnetization of the left half of the chain for  $L = 32$  sites and several values of  $\mu$ . Other parameters as in Fig. 3.

confirms our interpretation of a strongly interacting TRITOPS chain in terms of an effectively noninteracting TRITOPS with a renormalized parameter  $\Delta_s$ .

### C. Magnetic field at the end parallel to the SOC

For a very long chain in the regime  $L \gg \xi$ , and magnetic field parallel to the SOC, the system effectively behaves as if free fractionalized spins  $1/4$  existed at each end. This picture is based on the fact that an infinitesimally small  $J$  generates a magnetization  $\langle S_i^y \rangle = 1/4$ , where  $S_i^y = \sum_{i=1}^{L/2} S_i^y$  under a magnetic field  $-J \sum_{j=1}^{L/2} \mathbf{c}_j^\dagger \sigma_y \mathbf{c}_j$  applied to the left half of the chain [12,21,25]. On the other hand, for a finite noninteracting chain, due to the mixing of MZMs at the ends, the lowest-lying Kramers-degenerate one-particle excitations have a small but finite energy  $E(0)$  for  $J = 0$ , which decays exponentially with the length of the chain. For a finite Zeeman energy  $J$ , the Kramers degeneracy is broken and  $E(J)$ , which corresponds to  $E_1$  in Eq. (2), decreases.  $E(J)$  has been calculated analytically in Ref. [21], and the expectation value of the spin projection is described by the simple expression [21]

$$\langle S_i^y \rangle = \frac{2J_y}{4\sqrt{(2J_y)^2 + 16E(0)^2}}. \quad (3)$$

Therefore, the magnetization increases and saturates to the value  $1/4$  with an applied field, which is orders of magnitude

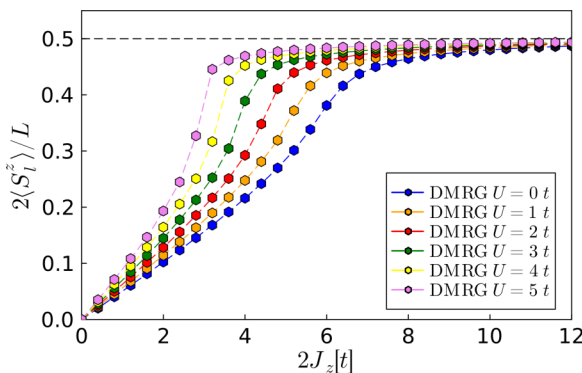


FIG. 5. Magnetization of the left half of the chain for  $L = 20$  sites and several values of  $U$ . Other parameters as in Fig. 3.

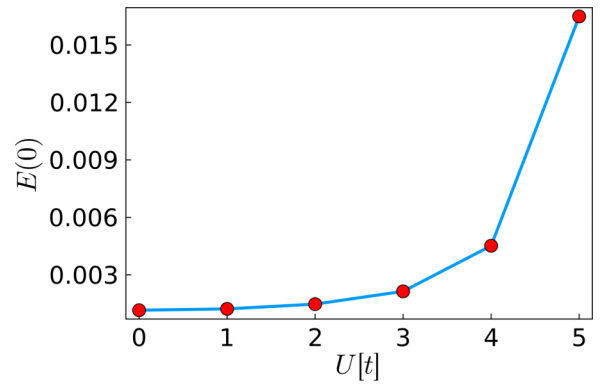


FIG. 6. Energy of the lowest one-particle excitation as function of  $U$  for a chain of  $L = 20$  sites. Other parameters as in Fig. 3.

smaller than in the case of a magnetic field perpendicular to the SOC discussed in Sec. III B.

In Fig. 6 we show the dependence of  $E(0)$  with  $U$ . The curve follows an exponential behavior with very small values for  $U \rightarrow 0$  and increases abruptly for  $U \sim 4$ . Again, this effect can be qualitatively explained in terms of a longer localization length  $\xi \sim \hbar v_F / \Delta_s$  due to the renormalization of  $\Delta_s$  to lower values by the effect of the interaction. Presumably, at the value of  $U \simeq 4$  the regime  $L \sim \xi$  is reached, and the mixing of MZMs at different ends becomes important. We illustrate this effect in Fig. 7, where we show the expectation value of the spin at each site for a chain of  $L = 20$  sites. Note that for  $U = 0$  and  $U = 2$  the expectation values of  $\langle S_i^y \rangle$  are localized near the ends and vanish exponentially fast near the middle of the chain. However, for  $U = 5$ , the magnetization is spread all over the system, indicating that the MZM localization length  $\xi$  is of the order of  $L$ .

Finally, in Fig. 8 we show the expectation value of the spin projection at the left end as a function of the magnetic field applied parallel to the SOC, for several values of  $U$ . Interestingly, note that despite the fact that Eq. (3) was analytically obtained for a noninteracting model, it remains valid even in the strongly-interacting regime (i.e., up to  $U \lesssim 3$ ) and shows universal behavior. Up to  $U \sim 5$  the expression is only qualitatively valid and it eventually breaks down for  $U > 7$ . This deviation and breakdown at extremely large values of  $U$  occurs because the MZMs (and therefore, the magnetization) are no longer localized at the ends, and the analytic approach of Ref. [21], which

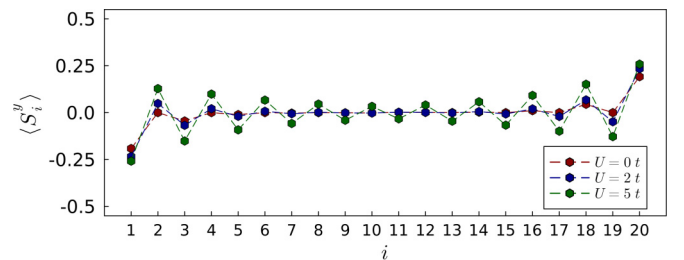


FIG. 7. Expectation value of the spin projection as a function of site for a chain of 20 sites,  $J_y = 10E(0)$  and different values of  $U$ . Other parameters as in Fig. 3.

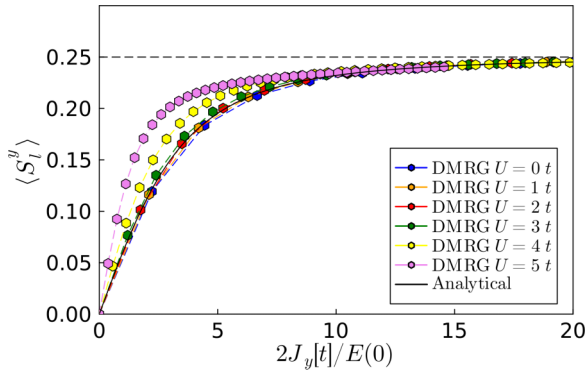


FIG. 8. Magnetization at the left side of the chain as a function of magnetic field applied to the left part of the chain for 20 sites and several values of  $U$ . Other parameters as in Fig. 3.

assumes localized zero-energy modes at the ends, is no longer valid.

#### IV. SUMMARY AND DISCUSSION

We have studied the strongly-interacting version of the one-dimensional Zhang-Kane-Mele model for time-reversal invariant topological superconductors. The model contains extended  $s$ -wave superconductivity and Rashba spin-orbit coupling (SOC) as key ingredients, and we incorporate an on-site Coulomb repulsion  $U$  and an external Zeeman field in order to study the stability of the TRITOPS phase and the emerging MZMs against the combined effects of the repulsive electron-electron interaction and the external field, which breaks the time-reversal symmetry. The model is relevant to understand the effect of repulsive interactions in different one-dimensional systems predicted to host TRITOPS phases, such as Shiba chains on top of high- $T_c$  superconductors [44].

By analyzing the degeneracy of the reduced density-matrix entanglement spectrum using the DMRG technique (as explained in Sec. III A), we have determined the different topological phases of the model as a function of chemical potential and magnetic field perpendicular to the SOC. Remarkably, the fourfold degeneracy characteristic of the TRITOPS phase remains stable up to quite large values of the external Zeeman field (i.e., comparable to the bandwidth). For larger values of the magnetic field only the twofold degenerate topological D phase and the trivial phase persist.

Concerning the effect of  $U$ , an important conclusion of this paper is that despite its effect on the topological phase diagram (i.e., redefining the topological phase boundaries), the presence of local repulsive interactions has no other qualitative effects. In fact, our results support a phenomenological picture where electron-electron interaction can be introduced in the renormalized parameters of an effectively noninteracting model. This has been confirmed by the fact that all physical properties seem to depend on the renormalized single-particle excitation gap  $\Delta_s$  (see Fig. 2). In few words, the interaction  $U$  weakens the fourfold degenerate phase against a perpendicular magnetic field, but it favors and stabilizes this phase with respect to a varying chemical potential. From a practical perspective, this last effect could be useful in potential appli-

cations in order to enlarge the range of chemical potential for which the topological phases exist.

We note that the persistence of the MZMs when the interaction is turned on, is not a general result. For example, in the interacting Su-Schrieffer-Heeger model, although in presence of the on-site repulsion  $U$ , two different topological sectors can still be identified by many-body topological invariants [46–48], the MZMs end states disappear even in the topological phase for finite  $U$  [47]. The presence of zero-energy edge modes dictated by the bulk-boundary correspondence is modified by the possible presence of zeros of the interacting Green’s function at zero energy [46,47,52]. Interestingly, a zero of this kind is responsible for a topological transition in a two-channel spin-1 Kondo model with easy-plane anisotropy [53], which explains several relevant experiments [53–55].

While at the moment there is no evidence, to our knowledge, of concrete experimental realizations of TRITOPS, the results found in this and other theoretical studies (see e.g., Ref. [44]) give hope in the search of potential realizations, in particular given the extended region of the fourfold degenerate phase in parameter space  $\mu$ - $J$  shown in Fig. 1, for different values of  $U$ . As mentioned before, a crucial aspect in the search of concrete realizations of TRITOPS is the presence of an extended superconducting pairing [14]. In this sense, superconductors with unconventional pairing symmetry are potential candidate materials. In particular, cuprate high- $T_c$  compounds, featuring  $d$ -wave pairing with nodal gapless points in the excitation spectrum, seems to be excluded in the search of potential TRITOPS platforms, as fully gapped systems are the obvious choice to obtain stable topological phases. This naturally narrows the search to the iron-pnictides and iron-chalcogenides superconductors, featuring an extended  $s$ -wave pairing with a fully gapped Fermi surface, such as FeSe [56,57], FeTeSe [58], LaFeAsO [59], and BaKFe<sub>2</sub>As<sub>2</sub> [60]. These materials have the additional advantage of having much larger  $T_c$  as compared to conventional  $s$ -wave materials, such as Al or Pb, typically used in different magnet/superconductor hybrid interfaces. We recall that a higher  $T_c$  usually indicates a larger gap size, a fact that simplifies the spectral resolution of subgap states and simultaneously enhances the topological protection of the MZMs [44]. Many other iron-based superconductors could be mentioned; however, in those cases the pairing symmetry is less clear and is currently under debate.

In order to characterize the different phases and the effect of the on-site interaction, we have calculated the magnetization at one end of the chain when a magnetic field is applied to that end. While external magnetic fields with atomic spatial resolution are not experimentally feasible, in the case of Shiba chains spin-polarized STM tips have allowed to study the spin response of atomic chains near the ends [61]. In our paper, we obtain a highly anisotropic response depending on the orientation of the externally applied field with respect to the SOC axis. For a magnetic field  $J$  parallel to the SOC, the spin projection at the end rapidly saturates [i.e., for field strengths corresponding to the small energy scale  $E(0)$  arising from mixing and energy splitting of the MZMs at different ends] to the unconventional value  $S = 1/4$ . This splitting decays exponentially with  $L$ , the length of the chain. For moderate values of  $U$ , the magnetization at the end follows a universal

curve as a function of the ratio between magnetic field and  $E(0)$  [see Eq. (3)].

For magnetic field perpendicular to the SOC, the magnetization at the end increases linearly with the applied field with a slope inversely proportional to the superconducting gap  $\Delta_s$ .

Finally, we comment on the possible effects of longer range repulsion. The effect of nearest-neighbor (long-range) repulsion on the Kitaev model has been studied by DMRG [62,63] (approximate [64]) methods. In addition, the effect of repulsions between a quantum dot and a Kitaev chain have been also studied [65,66]. From these papers we conclude that in order for these repulsive interactions to affect significantly the MZMs, they should reach simultaneously the MZMs of

both ends. In other words either the interactions are long range so that both MZMs repel each other, or the wire is sufficiently short so that there is a significant mixing between MZMs at both ends. We believe that this conclusion can be extended to our spinful model.

## ACKNOWLEDGMENTS

A.A.A. acknowledges financial support provided by PICT 2018-01546 and PICT 2020A-03661 of the Agencia I+D+i, Argentina. C.J.G. and L.M.C. acknowledge financial support provided by PIP 2021-3220 of CONICET. A.M.L. acknowledges financial support from Agencia I+D+i through Grant No. PICT 2017-2081.

- 
- [1] A. Y. Kitaev, Unpaired Majorana fermions in quantum wires, *Phys. Usp.* **44**, 131 (2001).
- [2] C. Nayak, S. H. Simon, A. Stern, M. Freedman, and S. Das Sarma, Non-Abelian anyons and topological quantum computation, *Rev. Mod. Phys.* **80**, 1083 (2008).
- [3] T. Giamarchi, *Quantum Physics in One Dimension* (Oxford University Press, Oxford, 2003).
- [4] G. Moore and N. Read, Nonabelions in the fractional quantum Hall effect, *Nucl. Phys. B* **360**, 362 (1991).
- [5] M. M. Salomaa and G. E. Volovik, Cosmiclike domain walls in superfluid  $^3B$ : Instantons and diabolical points in  $(k,r)$  space, *Phys. Rev. B* **37**, 9298 (1988).
- [6] L. Fu and C. L. Kane, Superconducting proximity effect and Majorana fermions at the surface of a topological insulator, *Phys. Rev. Lett.* **100**, 096407 (2008).
- [7] J. D. Sau, R. M. Lutchyn, S. Tewari, and S. Das Sarma, Generic new platform for topological quantum computation using semiconductor heterostructures, *Phys. Rev. Lett.* **104**, 040502 (2010).
- [8] R. M. Lutchyn, J. D. Sau, and S. Das Sarma, Majorana fermions and a topological phase transition in semiconductor-superconductor heterostructures, *Phys. Rev. Lett.* **105**, 077001 (2010).
- [9] Y. Oreg, G. Refael, and F. von Oppen, Helical liquids and Majorana bound states in quantum wires, *Phys. Rev. Lett.* **105**, 177002 (2010).
- [10] A. Altland and M. R. Zirnbauer, Nonstandard symmetry classes in mesoscopic normal-superconducting hybrid structures, *Phys. Rev. B* **55**, 1142 (1997).
- [11] S. Ryu, A. P. Schnyder, A. Furusaki, and A. W. W. Ludwig, Topological insulators and superconductors: Tenfold way and dimensional hierarchy, *New J. Phys.* **12**, 065010 (2010).
- [12] X.-L. Qi, T. L. Hughes, S. Raghu, and S.-C. Zhang, Time-reversal-invariant topological superconductors and superfluids in two and three dimensions, *Phys. Rev. Lett.* **102**, 187001 (2009).
- [13] X.-L. Qi, T. L. Hughes, and S.-C. Zhang, Topological invariants for the Fermi surface of a time-reversal-invariant superconductor, *Phys. Rev. B* **81**, 134508 (2010).
- [14] F. Zhang, C. L. Kane, and E. J. Mele, Time-reversal-invariant topological superconductivity and Majorana Kramers pairs, *Phys. Rev. Lett.* **111**, 056402 (2013).
- [15] S. Deng, L. Viola, and G. Ortiz, Majorana modes in time-reversal invariant  $s$ -wave topological superconductors, *Phys. Rev. Lett.* **108**, 036803 (2012).
- [16] E. Dumitrescu and S. Tewari, Topological properties of the time-reversal-symmetric Kitaev chain and applications to organic superconductors, *Phys. Rev. B* **88**, 220505(R) (2013).
- [17] A. Keselman, L. Fu, A. Stern, and E. Berg, Inducing time-reversal-invariant topological superconductivity and fermion parity pumping in quantum wires, *Phys. Rev. Lett.* **111**, 116402 (2013).
- [18] A. Haim, A. Keselman, E. Berg, and Y. Oreg, Time-reversal-invariant topological superconductivity induced by repulsive interactions in quantum wires, *Phys. Rev. B* **89**, 220504(R) (2014).
- [19] E. Mellars and B. Béri, Signatures of time-reversal-invariant topological superconductivity in the Josephson effect, *Phys. Rev. B* **94**, 174508 (2016).
- [20] A. Camjayi, L. Arrachea, A. Aligia, and F. von Oppen, Fractional spin and Josephson effect in time-reversal-invariant topological superconductors, *Phys. Rev. Lett.* **119**, 046801 (2017).
- [21] A. A. Aligia and L. Arrachea, Entangled end states with fractionalized spin projection in a time-reversal-invariant topological superconducting wire, *Phys. Rev. B* **98**, 174507 (2018).
- [22] C. Schrade and L. Fu, Parity-controlled  $2\pi$  Josephson effect mediated by Majorana Kramers pairs, *Phys. Rev. Lett.* **120**, 267002 (2018).
- [23] L. Arrachea, A. Camjayi, A. A. Aligia, and L. Grunfeiro, Catalog of Andreev spectra and Josephson effects in structures with time-reversal-invariant topological superconductor wires, *Phys. Rev. B* **99**, 085431 (2019).
- [24] O. E. Casas, L. Arrachea, W. J. Herrera, and A. L. Yeyati, Proximity induced time-reversal topological superconductivity in  $\text{Bi}_2\text{Se}_3$  films without phase tuning, *Phys. Rev. B* **99**, 161301(R) (2019).
- [25] A. A. Aligia and A. Camjayi, Exact analytical solution of a time-reversal-invariant topological superconducting wire, *Phys. Rev. B* **100**, 115413 (2019).
- [26] A. Haim and Y. Oreg, Time-reversal-invariant topological superconductivity in one and two dimensions, *Phys. Rep.* **825**, 1 (2019).
- [27] S. V. Aksenov, A. O. Zlotnikov, and M. S. Shustin, Strong Coulomb interactions in the problem of Majorana modes in a

- wire of the nontrivial topological class BDI, *Phys. Rev. B* **101**, 125431 (2020).
- [28] M. S. Shustin and S. V. Aksenov, Features of physical observables of a strongly correlated superconducting nanowire with Rashba spin-orbit interaction, *J. Exp. Theor. Phys.* **135**, 500 (2022).
- [29] G. F. R. Ruiz, M. A. Rampp, A. A. Aligia, J. Schmalian, and L. Arrachea, Josephson junctions of two-dimensional time-reversal invariant superconductors: Signatures of the topological phase, *Phys. Rev. B* **106**, 195415 (2022).
- [30] J. Danon and K. Flensberg, Interaction effects on proximity-induced superconductivity in semiconducting nanowires, *Phys. Rev. B* **91**, 165425 (2015).
- [31] A. Haim, K. Wölms, E. Berg, Y. Oreg, and K. Flensberg, Interaction-driven topological superconductivity in one dimension, *Phys. Rev. B* **94**, 115124 (2016).
- [32] X.-R. Ma, W. Li, Z.-H. Yuan, W.-H. Zhou, N. Nan, D.-F. Chen, Y.-D. Hou, J. Zhang, and Y.-C. Xiong, Yu-Shiba-Rusinov states assisted by asymmetric Coulomb repulsion in a bipartite molecular device, *J. Phys.: Condens. Matter* **35**, 445001 (2023).
- [33] S. Gangadharaiah, B. Braunecker, P. Simon, and D. Loss, Majorana edge states in interacting one-dimensional systems, *Phys. Rev. Lett.* **107**, 036801 (2011).
- [34] A. M. Lobos, R. M. Lutchyn, and S. Das Sarma, Interplay of disorder and interaction in Majorana quantum wires, *Phys. Rev. Lett.* **109**, 146403 (2012).
- [35] K. Sun, C.-K. Chiu, H.-H. Hung, and J. Wu, Tuning between singlet, triplet, and mixed pairing states in an extended Hubbard chain, *Phys. Rev. B* **89**, 104519 (2014).
- [36] A. Keselman and E. Berg, Gapless symmetry-protected topological phase of fermions in one dimension, *Phys. Rev. B* **91**, 235309 (2015).
- [37] S. Nadj-Perge, I. K. Drozdov, B. A. Bernevig, and A. Yazdani, Proposal for realizing Majorana fermions in chains of magnetic atoms on a superconductor, *Phys. Rev. B* **88**, 020407(R) (2013).
- [38] J. Klinovaja, P. Stano, A. Yazdani, and D. Loss, Topological superconductivity and Majorana fermions in RKKY systems, *Phys. Rev. Lett.* **111**, 186805 (2013).
- [39] B. Braunecker and P. Simon, Interplay between classical magnetic moments and superconductivity in quantum one-dimensional conductors: Toward a self-sustained topological Majorana phase, *Phys. Rev. Lett.* **111**, 147202 (2013).
- [40] S. Nadj-Perge, I. K. Drozdov, J. Li, H. Chen, S. Jeon, J. Seo, A. H. MacDonald, B. A. Bernevig, and A. Yazdani, Observation of Majorana fermions in ferromagnetic atomic chains on a superconductor, *Science* **346**, 602 (2014).
- [41] M. Ruby, F. Pientka, Y. Peng, F. von Oppen, B. W. Heinrich, and K. J. Franke, End states and subgap structure in proximity-coupled chains of magnetic adatoms, *Phys. Rev. Lett.* **115**, 197204 (2015).
- [42] R. Pawlak, M. Kisiel, J. Klinovaja, T. Meier, S. Kawai, T. Glatzel, D. Loss, and E. Meyer, Probing atomic structure and Majorana wavefunctions in mono-atomic Fe chains on superconducting Pb surface, *npj Quantum Inf.* **2**, 16035 (2016).
- [43] H. Kim, A. Palacio-Morales, T. Posske, L. Rózsa, K. Palotás, L. Szunyogh, M. Thorwart, and R. Wiesendanger, Toward tailoring Majorana bound states in artificially constructed magnetic atom chains on elemental superconductors, *Sci. Adv.* **4**, aar5251 (2018).
- [44] D. Crawford, E. Mascot, D. K. Morr, and S. Rachel, High-temperature Majorana fermions in magnet-superconductor hybrid systems, *Phys. Rev. B* **101**, 174510 (2020).
- [45] M. Fishman, S. R. White, and E. M. Stoudenmire, The ITensor software library for tensor network calculations, *SciPost Phys. Codebases* **4** (2022).
- [46] V. Gurarie, Single-particle Green's functions and interacting topological insulators, *Phys. Rev. B* **83**, 085426 (2011).
- [47] S. R. Manmana, A. M. Essin, R. M. Noack, and V. Gurarie, Topological invariants and interacting one-dimensional fermionic systems, *Phys. Rev. B* **86**, 205119 (2012).
- [48] A. A. Aligia, Topological invariants based on generalized position operators and application to the interacting Rice-Mele model, *Phys. Rev. B* **107**, 075153 (2023).
- [49] F. Pollmann, A. M. Turner, E. Berg, and M. Oshikawa, Entanglement spectrum of a topological phase in one dimension, *Phys. Rev. B* **81**, 064439 (2010).
- [50] A. M. Turner, F. Pollmann, and E. Berg, Topological phases of one-dimensional fermions: An entanglement point of view, *Phys. Rev. B* **83**, 075102 (2011).
- [51] E. Dumitrescu, J. D. Sau, and S. Tewari, Magnetic field response and chiral symmetry of time-reversal-invariant topological superconductors, *Phys. Rev. B* **90**, 245438 (2014).
- [52] L. P. Gavensky, S. Sachdev, and N. Goldman, Connecting the many-body Chern number to Luttinger's theorem through Sřředa's formula, *Phys. Rev. Lett.* **131**, 236601 (2023).
- [53] R. Žitko, G. G. Blesio, L. O. Manuel, and A. A. Aligia, Iron phthalocyanine on Au(111) is a "non-Landau" Fermi liquid, *Nat. Commun.* **12**, 6027 (2021).
- [54] G. G. Blesio, R. Žitko, L. O. Manuel, and A. A. Aligia, Topological quantum phase transition of nickelocene on Cu(100), *SciPost Phys.* **14**, 042 (2023).
- [55] G. G. Blesio and A. A. Aligia, Topological quantum phase transition in individual Fe atoms on MoS<sub>2</sub>/Au(111), *Phys. Rev. B* **108**, 045113 (2023).
- [56] F.-C. Hsu, J.-Y. Luo, K.-W. Yeh, T.-K. Chen, T.-W. Huang, P. M. Wu, Y.-C. Lee, Y.-L. Huang, Y.-Y. Chu *et al.*, Superconductivity in the PbO-type structure  $\alpha$ -FeSe, *Proc. Natl. Acad. Sci. USA* **105**, 14262 (2008).
- [57] S. Medvedev, T. M. McQueen, I. A. Troyan, T. Palasyuk, M. I. Eremets, R. J. Cava, S. Naghavi, F. Casper, V. Ksenofontov, G. Wortmann, and C. Felser, Electronic and magnetic phase diagram of  $\beta$ -Fe1.01Se with superconductivity at 36.7 K under pressure, *Nat. Mater.* **8**, 630 (2009).
- [58] D. Wang, L. Kong, P. Fan, H. Chen, S. Zhu, W. Liu, L. Cao, Y. Sun, S. Du, J. Schneeloch *et al.*, Evidence for Majorana bound states in an iron-based superconductor, *Science* **362**, 333 (2018).
- [59] K. Kuroki, S. Onari, R. Arita, H. Usui, Y. Tanaka, H. Kontani, and H. Aoki, Unconventional pairing originating from the disconnected Fermi surfaces of superconducting LaFeAsO<sub>1-x</sub>F<sub>x</sub>, *Phys. Rev. Lett.* **101**, 087004 (2008).
- [60] J. Li, P. J. Pereira, J. Yuan, Y.-Y. Lv, M.-P. Jiang, D. Lu, Z.-Q. Lin, Y.-J. Liu, J.-F. Wang, L. Li *et al.*, Nematic superconducting state in iron pnictide superconductors, *Nat. Commun.* **8**, 1880 (2017).
- [61] S. Jeon, Y. Xie, J. Li, Z. Wang, B. A. Bernevig, and A. Yazdani, Distinguishing a Majorana zero mode using spin-resolved measurements, *Science* **358**, 772 (2017).



- [62] R. Thomale, S. Rachel, and P. Schmitteckert, Tunneling spectra simulation of interacting Majorana wires, *Phys. Rev. B* **88**, 161103(R) (2013).
- [63] N. M. Gergs, L. Fritz, and D. Schuricht, Topological order in the Kitaev/Majorana chain in the presence of disorder and interactions, *Phys. Rev. B* **93**, 075129 (2016).
- [64] A. Więckowski and A. Ptok, Influence of long-range interaction on Majorana zero modes, *Phys. Rev. B* **100**, 144510 (2019).
- [65] L. S. Ricco, Y. Marques, J. E. Sanches, I. A. Shelykh, and A. C. Seridonio, Interaction induced hybridization of Majorana zero modes in a coupled quantum-dot–superconducting-nanowire hybrid system, *Phys. Rev. B* **102**, 165104 (2020).
- [66] R. K. Takagui-Perez and A. Aligia, Effect of interatomic repulsion on Majorana zero modes in a coupled quantum-dot–superconducting-nanowire hybrid system, [arXiv:2309.10888](https://arxiv.org/abs/2309.10888).